The retrieval of cloud properties based on spectral solar light diffuse transmittance measurements under optically thick cloud cover conditions

A.A. Kokhanovsky [a,*], A. Smirnov [b,c], S.V. Korkin [d], G. Wind [b,e], I. Slutsker [b,c]

[a] VITROCISET Belgium SPRL, A Leonardo Company, Bratustrasse 7, 64295 Darmstadt, Germany
[b] Science Systems and Applications, Inc., Lanham, MD 20706 USA
[c] Biospheric Sciences Laboratory, NASA Goddard Space Flight Center, Greenbelt, MD 20771 USA
[d] USRA GESTAR, 7178 Columbia Gateway Drive, Columbia, Maryland 21046 USA
[e] Atmospheric Sciences Laboratory, NASA GSFC, Greenbelt, Maryland, USA

ARTICLE INFO

ABSTRACT

We propose a simple and fast cloud retrieval technique based on the spectral diffuse transmittance measurements under optically thick clouds. The technique is aimed at retrieval of cloud optical thickness, liquid water path and effective radius of particles in cloudy media. It is based on the asymptotic radiative transfer solutions valid at cloud optical thicknesses above 10. Also we use the parametrizations of the Mie theory results for local optical properties of clouds such as the single scattering albedo, extinction coefficient, and asymmetry parameter. This makes it possible to reduce the inverse problem solution to finding a root of a simple transcendent equation.

1. Introduction

Cloud properties such as cloud optical thickness and effective radius of particles at a given location can change rapidly with time due to various dynamical, thermodynamical and aerosol-cloud interaction processes. Polar orbiting satellites observe cloud properties outside polar regions a very limited number of times per day [1]. Therefore, the cloud diurnal cycle at a given location can not be studied unless the location is a polar one. The geostationary systems have much better temporal sampling outside polar regions (1–2 km spatial resolution with typically 5–15 min sampling) . However, the derived information is not always sufficient for understanding physical processes occurring within cloud systems on fine spatial and temporal scales. Satellite observations are well suited for the observations of cloud parameters at cloud tops. The information on the cloud properties (say, the shape and size of particles) at cloud base is hardly accessible by satellite systems. Therefore, a number of techniques had been developed for the de-

termination of cloud properties using ground-based and shipborne observations [2–15].

The diffuse radiation transmission function in the visible light is not a monotonic function of the cloud optical thickness (COT) [8]. Initially it increases with COT (outside the direction towards the Sun, where one must account also for the direct light). However, it decreases monotonically with the cloud optical thickness in the diffuse scattering regime occurring for clouds with COT above 5.0 or so [8]. Such clouds can be readily recognized by the absence of increased light intensity in the direction of Sun and also by the cosine law for angular distribution of intensity of diffuse radiation measured in the principal plane. The almucantar measurements can be also used to distinguish the diffuse scattering regime because for thick clouds there is no azimuthal dependence in the transmitted radiation.

In this paper we propose a simple and fast technique to determine the cloud optical thickness from cloud diffuse radiation transmittance measurements in the visible. The diffuse radiation transmittance in the visible also slightly depends on the size of particles in clouds. Therefore, we determine the effective radius (ER) a_{ef} (defined as the ratio of the third to the second moment of the droplet size distribution) of particles in clouds from the

near-infrared measurements. This makes it possible to derive COT with higher accuracy and also determine the liquid/ice water path. The technique is valid for optically thick horizontally homogeneous cloud systems. Therefore, the broken cloud fields are out of scope of this research. The vertical inhomogeneity of clouds does not present a serious obstacle to application of the developed technique for the determination of the cloud optical thickness because the profiles of liquid/ice water content and effective size of particles in clouds only weakly influence the cloud transmittance function in the visible. The retrievals of liquid water path and effective radius are affected by the vertical cloud inhomogeneity. The most accurate retrievals of these parameters are obtained for the case of clouds with weak vertical inhomogeneity. The technique is applied to AERONET [16] observations of a cloud field at the GSFC AERONET site (USA) and compared to the retrievals of cloud optical thickness as performed using standard AERONET cloud retrieval mode [9,10].

2. Theory

2.1. Retrieval of cloud optical thickness

The cloud bidirectional transmittance factor (BTF) or transmission function is defined as

$$T = \frac{\pi I}{\mu_0 F_0}, \tag{1}$$

where I is the transmitted diffuse light intensity, μ_0 is the cosine of the solar zenith angle (SZA), F_0 is the extraterrestrial solar irradiance at a given wavelength. The BTF is related to the cloud transport optical thickness τ_{tr} by the following equation in the case of nonabsorbing clouds [12,17]:

$$T = tu(\mu_0)u(\mu), \tag{2}$$

where the global transmittance

$$t = \frac{1}{a + b\,\tau_{tr}}, \tag{3}$$

$a = 1.072$, $b = 0.75$, μ is the cosine of the viewing zenith angle. The transport (reduced) cloud thickness is defined as: $\tau_{tr} = (1 - g)\tau$, where g is the asymmetry parameter (average cosine of scattering angle) and τ is the cloud optical thickness (COT). The angular function $u(\mu)$ can be derived using the following approximation [12,18]:

$$u(\mu) = \frac{3}{7}[1 + 2\mu]. \tag{4}$$

The accuracy of Eq. (2) with accounting for Eqs. (3) and (4) is high at values of τ_{tr} larger than 2.0 as demonstrated in Fig. 1, where the inverse value of BTF is shown as function of the scaled optical thickness at the solar zenith angle equal to 60° and zenith observations for two values of asymmetry parameter $g = 0.75$ (typical for ice clouds), 0.85 (typical for water clouds). The calculations have been performed using simple analytical Eqs. (1-4) and also using the integro - differential radiative transfer (RT) equation [18]. In particular, the exact radiative transfer results shown in Fig. 1 have been derived using the code IPOL (Intensity and POLarization) [19] for the Henyey – Greenstein phase function [20] at COTs in the range 1–100. IPOL is a Fortran 90/95, BLAS/LAPACK based, discrete-ordinates matrix-operator radiative transfer code. It is used for numerical simulation of monochromatic solar light scattering in a plane-parallel turbid media bounded from below by a reflecting surface. For faster convergence of the azimuth (Fourier) expansion, IPOL computes the first scattering order analytically, which is a standard technique. However, truncation of the phase function is not used since
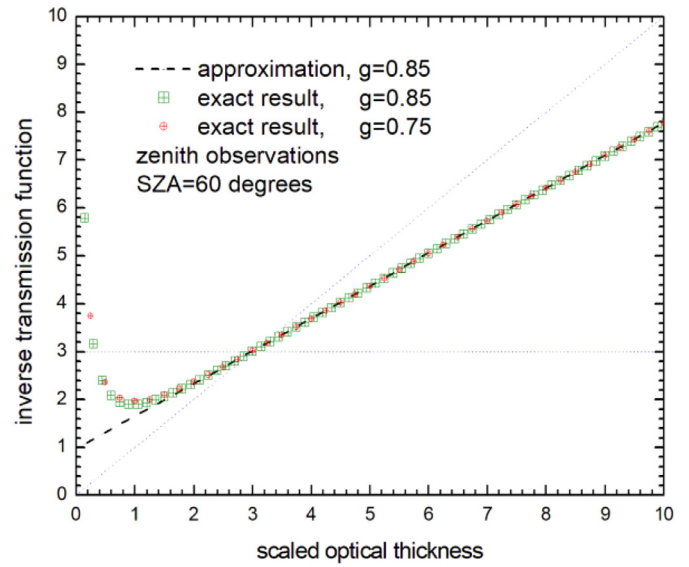
Fig. 1. The dependence of the inverse value of the BTF on the scaled optical thickness calculated using Eqs. (2) - (4) and the radiative transfer code IPOL at single scattering albedo $\omega_0 = 1$, the Henyey - Greenstein phase function and two values of the asymmetry parameter (0.75, 0.85) at the zenith direction. The solar zenith angle is equal to 60°.
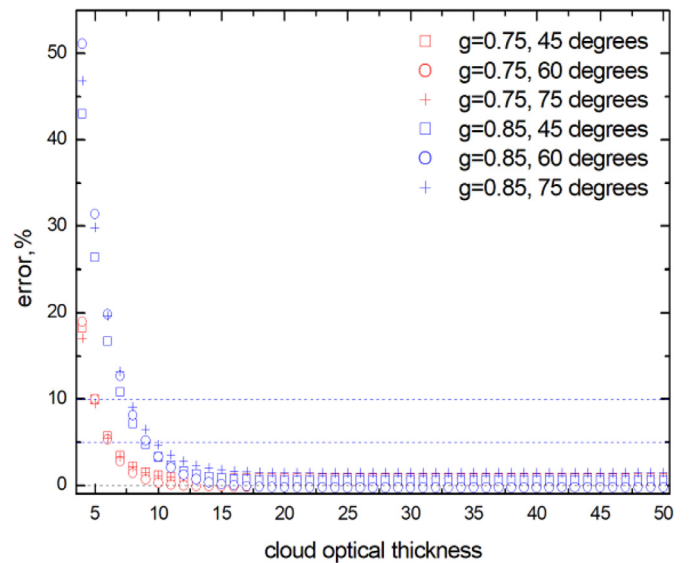
Fig. 2. The dependence of the relative error of the cloud BTF given by Eq. (2) on the cloud optical thickness at $g = 0.75$, 0.85 in the absence of absorption in clouds. The Henyey-Greenstein phase function has been assumed. The solar zenith angle is 54, 60, and 75°. The observation is in the zenith direction.

it spoils transmittance in the aureole [21]. Recent RT codes intercomparison in a variety of scenarios indicated that numerical error of IPOL is at or below 0.1% including the aureole [22]. It follows that the relative error of Eq. (2) (with account for Eqs. (3), (4)) is small at τ_{tr} larger than 2. It is interesting to note that the dependence of T on the scaled optical thickness (and not separately on g and τ) is valid in a broader range of τ_{tr} as compared to the range of validity of Eq. (2). The dependence of relative error of Eq. (2) with account for Eqs. (3) and (4) on the value of τ_{tr} is given in Fig. 2 for various solar zenith angles. One concludes that the error is smaller than 5% at $COT \geq 10\,(7)$ for water(ice)clouds. The smaller error for ice clouds is explained by the fact that the transport optical thickness is larger for ice clouds (for the same value of COT) and equations have better accuracy for larger values of τ_{tr}

(see Fig. 1). The error of Eq. (2) is below 1–2% at COTs above 15, which is smaller as compared to the measurement error.

Therefore, we conclude that Eq. (2) can be used to derive the cloud transport optical thickness via the following simple relationship:

$$\tau_{tr} = \frac{1}{b}\left[\frac{u(\mu_0)u(\mu)}{T} - a\right]. \tag{5}$$

Taking into account that $\tau_{tr} = (1 - g)\tau$, one can easily derive cloud optical thickness τ in case the asymmetry parameter g is known in advance or assumed. Usually it is assumed that $g = 0.75$ for ice clouds and it is equal to 0.85 for water clouds. Uncertainty in the value of g introduces biases in the retrieved value of COT:

$$\tau = \frac{1}{\gamma b}\left[\frac{u(\mu_0)u(\mu)}{T} - a\right], \tag{6}$$

where $\gamma = 1 - g$ is the symmetry parameter. Note that γ is equal to 1 for the isotropic and Rayleigh scattering cases.

The absolute error in the retrieved COT can be presented in the following way:

$$\Delta\tau = \sqrt{k_1^2(\Delta T)^2 + k_2^2(\Delta\gamma)^2}, \tag{7}$$

where we ignore an error related to uncertainty in the angular function. The value of ΔT is the absolute error of the measured diffuse transmittance, $\Delta\gamma$ is the absolute uncertainty in the symmetry parameter and

$$k_1 = \frac{\partial\tau}{\partial T}, \quad k_2 = \frac{\partial\tau}{\partial\gamma}. \tag{8}$$

These derivatives can be derived analytically:

$$k_1 = -\frac{a + b\gamma\tau}{b\gamma T}, \quad k_2 = -\frac{\tau}{\gamma}. \tag{9}$$

If the value of the symmetry parameter γ is known without any bias, then one can derive:

$$\frac{\Delta\tau}{\tau} = \epsilon\frac{\Delta T}{T}, \tag{10}$$

where $\epsilon = -1 - \frac{a}{b\gamma\tau}$. It follows that ϵ is close to -1 for large values of τ. This means that the error in the retrieved value of COT is approximately equal to the error of the measured transmittance. Therefore, there is no large error enhancement.

2.2. Retrieval of liquid water path and effective size of particles in clouds

2.2.1. The direct problem: the parameterization of the bidirectional transmission function with respect to liquid water path and effective size of particles

The retrieval of COT discussed above can be biased because dependence of the asymmetry parameter on size and shape of particles is ignored. Although these effects can be neglected for the procedure of scaled optical thickness determination. Because the radiative budget under clouds is governed by τ_{tr} (see Eq. (3)) and the reduced COT is less influenced by cloud microstructure, the value of τ_{tr} must be reported in output of cloud retrieval algorithms whenever it is possible.

The accuracy of COT retrievals (especially for water clouds) can be increased, if the size of particles is determined from the cloud BTF in the shortwave infrared (SWIR). The single scattering albedo ω_0 differs from unity in the SWIR and depends on the size of particles because condensed water absorbs incoming light in SWIR. The absorption is generally stronger for larger particles. This leads to increase of cloud absorptance and decrease of transmittance with the size of particles (at fixed g). On the other hand, the asymmetry parameter increases with the size of particles. This leads to decrease of the scaled COT and increase of the BTF at fixed absorption. These two different tendencies lead to nonmonotonic behavior of the function $T(a_{ef})$. Therefore, the determination of the effective radius from spectral BTF is not straightforward and multiple solutions of inverse problem are possible. For sufficiently large particles it follows that T is a decreasing function of a_{ef} (in water absorption bands) [8]. The opposite is true at the single scattering albedo (SSA) $\omega_0 = 1$ because, clouds with larger particles are characterized generally by the smaller reduced COT.

The value of ω_0 is close to 1.0 for clouds in the near IR and SWIR [17]. Then it follows for the BTF [12,17]:

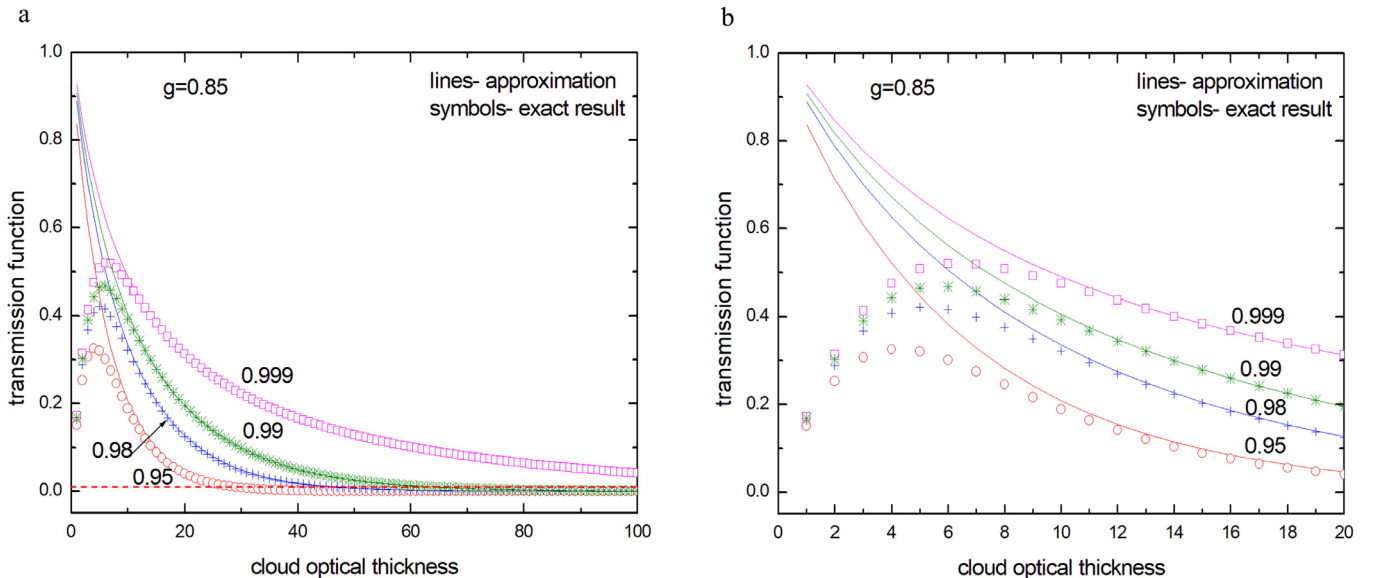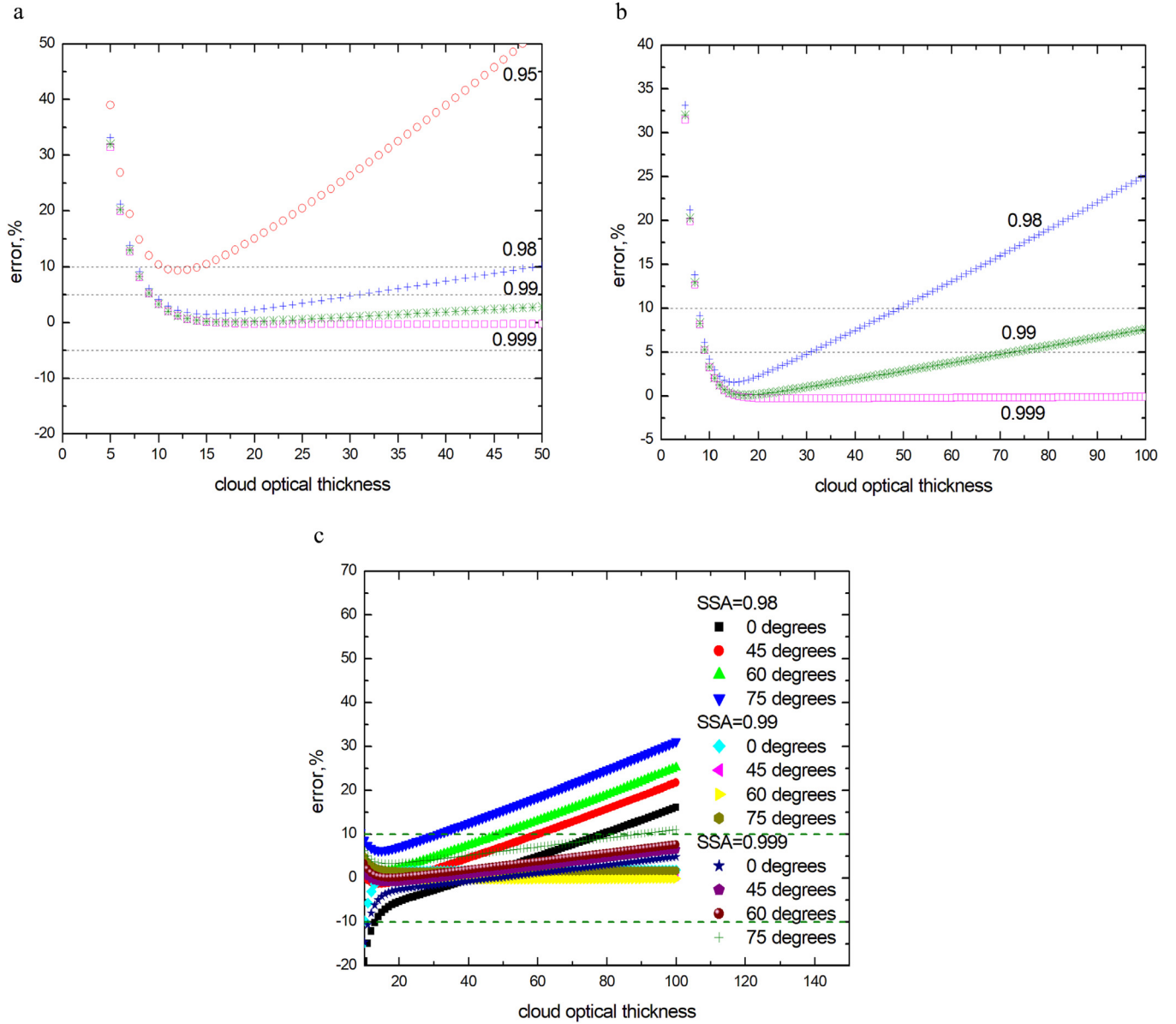$$T = \frac{u(\mu_0)u(\mu)\sinh(y)}{\sinh(x + ay)}, \tag{11}$$

a

b

Fig. 3. a. The dependence of transmission function on cloud optical thickness at several values of SSA, zenith observations and solar zenith angle 60° (symbols- exact calculations using Henyey – Greenstein phase function with $g = 0.85$; lines- Eq. (11)). b. The same as in Fig. 3a except for a smaller range of COTs.

a

b

c

Fig. 4. a. The relative error of Eq. (11) as function of cloud optical thickness at several values of SSA. Other parameters used in calculations are the same as in Fig. 3a. b. The same as in Fig. 4a but for larger range of COTs. The results for the case of 0.95 are not shown because such values of SSA do not occur in nonprecipitating clouds. c. The dependence of relative error of Eq. (11) on COT for various values of SSA and SZA.

where

$$x = \kappa\tau, y = 4\sqrt{\frac{\beta}{3\gamma}}, \tag{12}$$

$\kappa = \sqrt{3\beta\gamma}$ is the diffusion exponent and $\beta = 1 - \omega_0$ is the probability of photon absorption. We also can write: $y = \frac{4\kappa}{3\gamma}$. Eq. (2) follows from Eq. (11) at $\omega_0 = 1$ [17]. The accuracy of Eq. (11) is presented in Figs. 3 and 4. It follows that the error of approximations is below 10% at SSA smaller than 0.98 (characteristic for non-precipitating clouds) and COT in the range 8–50. The errors for larger COTs are also small at SSA below 0.99. The relative error of the approximations at larger values of SSA increases because $t \to 0$ in the case of thick absorbing clouds. Then the measurements are accompanied by larger experimental errors and noise, which makes the cloud property retrievals not reliable anyway.

The diffusion exponent κ and also the similarity parameter y (see Eq. (12)) depend on the size of particles. We have found that

Table 1
The parameters of the fitting function (13). The refractive index of water used in Mie calculations was 1.3085+0.000079i (at the wavelength 1640 nm).

f	c_0	c_1	c_2	v_1, 1/μm	v_2, 1/μm
κ	0.03394	0.04652	0.07901	0.10645	0.01522
y	0.17267	1.20144	0.72656	0.01466	0.10401

they can be approximated by the following function:

$$f = c_0 + c_1 \exp\left(-\frac{1}{v_1 a_{ef}}\right) + c_2 \exp\left(-\frac{1}{v_2 a_{ef}}\right), \tag{13}$$

where a_{ef} is in microns. The coefficients of this function, listed in Table 1, have been calculated using Mie theory at the refractive index 1.3085+0.000079i (at 1640 nm) for the droplet size distri-

a

b
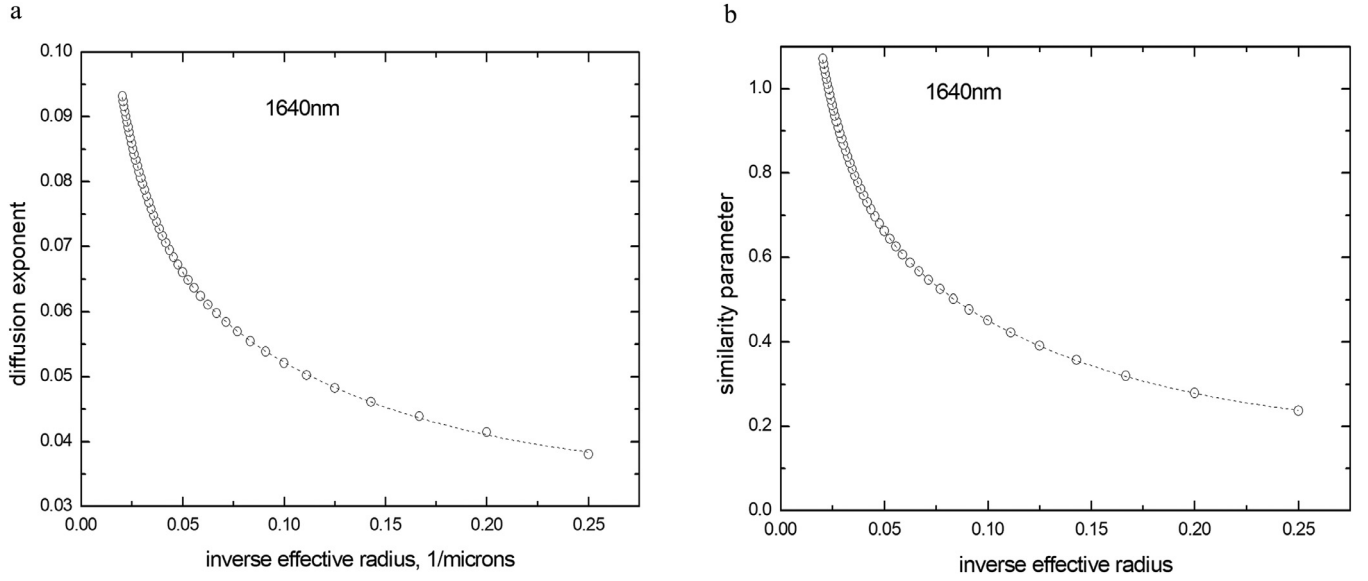
Fig. 5. a. The diffusion exponent as function of the inverse effective radius of droplets. b. The similarity parameter as function of the inverse effective radius of droplets.

bution:

$$\varphi(a) = D\left(\frac{a}{a_0}\right)^6 \exp\left(-\frac{6a}{a_0}\right), \tag{14}$$

where $D = \frac{6^5}{140a_0}$, $a_0 = \frac{2a_{ef}}{3}$ is the mode radius. The accuracy of fitting is shown in Fig. 5 as the function of inverse effective radius of droplets.

The cloud optical thickness also depends on the effective radius. It can be presented as product of the cloud extinction coefficient and a cloud geometrical thickness L:

$$\tau = k_{ext}L, \tag{15}$$

where it follows in the geometrical optics approximation:

$$k_{ext} = \frac{3C}{2a_{ef}}, \tag{16}$$

where C is the volumetric concentration of droplets. Let us introduce the normalized extinction coefficient:

$$K = \frac{k_{ext}}{C} \tag{17}$$

and the liquid water path (LWP):

$$W = C\rho L, \tag{18}$$

where ρ is the density of water. Then it follows:

$$\tau = KW/\rho. \tag{19}$$

The normalized extinction coefficient can be approximated by the following equation:

$$K = \frac{3}{2a_{ef}}\left(1 + \frac{\upsilon}{x_{ef}^{\frac{2}{3}}} + \frac{\varsigma}{x_{ef}^{\frac{4}{3}}}\right), \tag{20}$$

where $x_{ef} = ka_{ef}$, $k = 2\pi/\lambda$, λ is the wavelength, $\upsilon = 1.1$, $\varsigma = 4.8$. The pair (υ, ς) has been derived fitting Eq. (20) to the results of Mie calculations. It should be noted that Eq. (20) provides correct geometrical optics result ($K = 1.5/a_{ef}$) as $x_{ef} \to \infty$. The accuracy of Eq. (20) is shown in Fig. 6 at the wavelengths 440 and 1600 nm. We have assumed that water clouds do not absorb radiation at 440 nm and the real part of water refractive index is 1.345. It follows that Eq. (20) is very accurate at both wavelengths for the
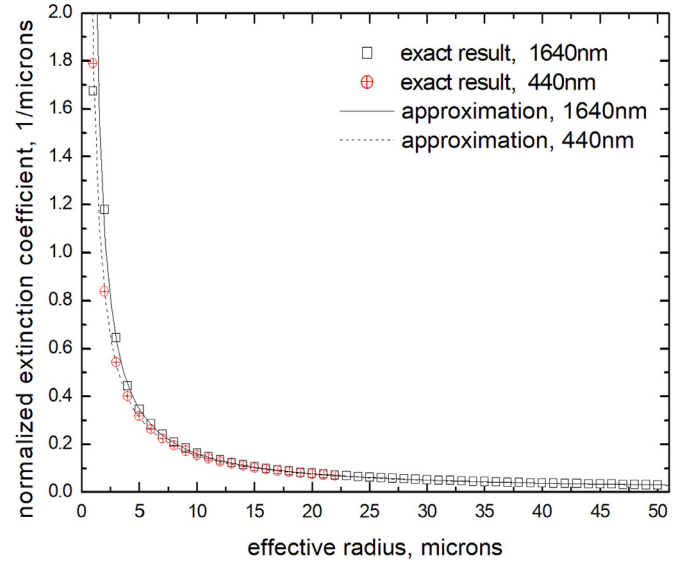
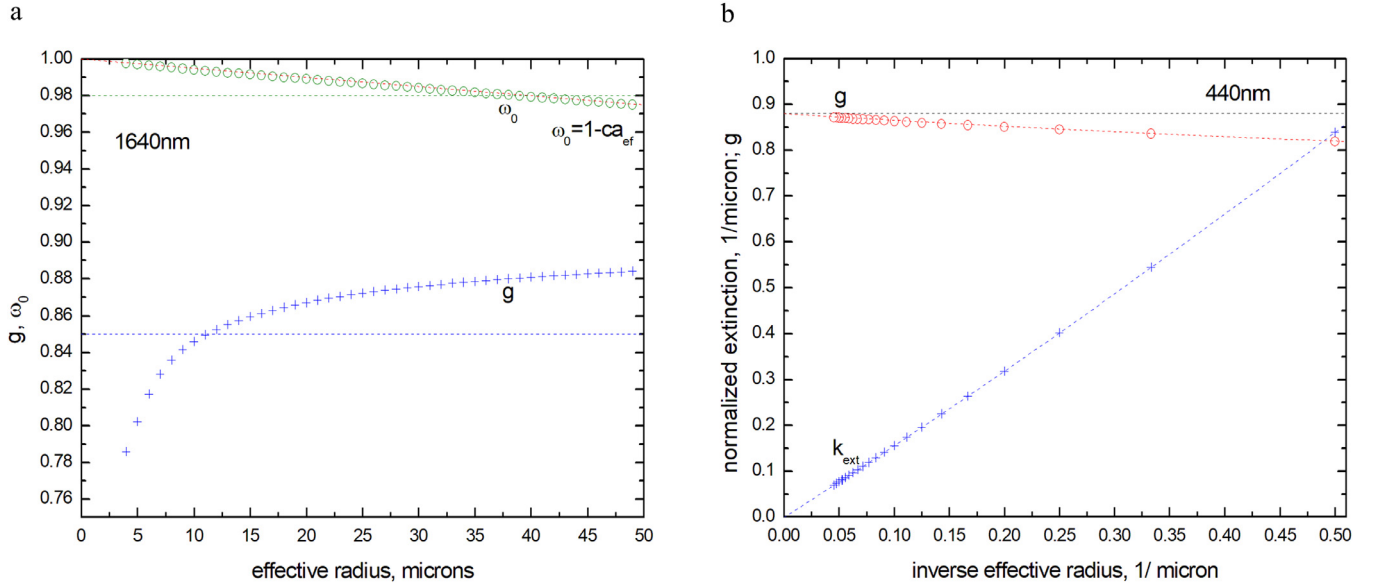**Fig. 6.** The normalized cloud extinction coefficient at 1640 nm.

range of effective radii common in water clouds. For completeness, we also show the dependence of the parameters of g, ω_0 at 1640 nm and the parameters g, K at 440 nm as functions of a_{ef} in Fig. 7. We note that the asymmetry parameter does not deviate significantly from the value $g = 0.85$ used in the studies of the accuracy of the approximation presented above. It can be approximated by the following analytical function at 440nm:

$$g = 0.88 - \frac{2.14}{x_{ef}} + \frac{10.2}{x_{ef}^2}, \tag{21}$$

Also, as it follows from Fig. 7a, the value of ω_0 is larger than 0.99 at 1640 nm for the range of radii usually occurring in non-precipitating clouds and $1-\omega_0$ is linearly proportional to a_{ef} in the range of droplet radii characteristic for nonprecipitating clouds. Namely in this range the error of the analytical equations for the cloud transmission function presented here is the smallest one.

The analytical equations presented above can be used for the solution of both direct and inverse problems of cloud optics. In

a

b

Fig. 7. a. The asymmetry parameter and single scattering albedo of water clouds calculated using Mie theory at 1640 nm. The parameter c is equal to 0.0005 μm^{-1}. b. The asymmetry parameter and normalized extinction coefficient of water clouds calculated using Mie theory at 440 nm.
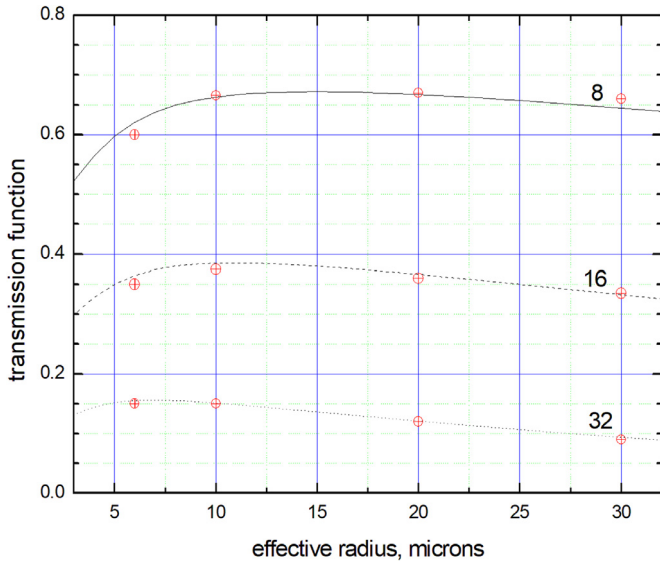
Fig. 8. The dependence of the transmission function on the effective radius of particles calculated using Eq. (12) (lines) and exact radiative transfer [7] at COTs (500 nm) equal to 8, 16, and 32 (SZA=30° and VZA=0°) .
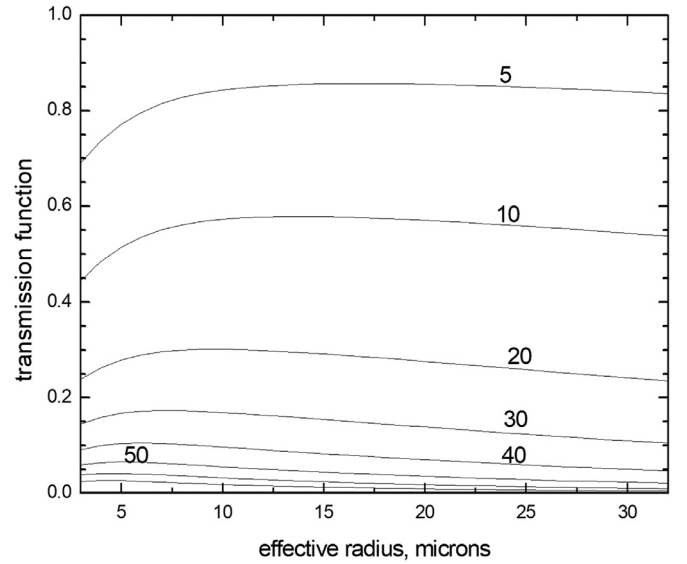
Fig. 9. The dependence of the transmission function on the effective radius of particles calculated using Eq. (12) (lines) at COTs (500 nm) equal to 5, 10(10)70 (SZA=30° and VZA=0°) .

particular, we show the dependence of the transmission function on the effective radius of droplets calculated using Eq. (12) and exact radiative transfer calculations at COTs (500 nm) equal to 8, 16, and 32, SZA=30°, VZA=0° in Fig. 8. It follows that the accuracy of the parametrization is accurate enough for the solution of both direct and inverse problems of cloud optics. The accuracy increases with the size of particles and COT.

It follows that for a given value of the transmission function, multiple solutions for the value of effective radius are possible (see also Fig. 9). To avoid this problem, one needs to use spectral measurements and not measurements at just two wavelengths (say, at 440 and 1640 nm).

2.2.2. The inverse problem

2.2.2.1. The solution of inverse problem for underlying black surface. The retrieval of the parameters a_{ef} and W can be performed in a

way as described below. First of all LWP can be expressed via the cloud optical thickness in the visible:

$$W = \frac{\rho \tau (440nm)}{K}, \tag{22}$$

where K is given by Eq. (20) and $\tau(440nm)$ is given by Eq. (6) with account for Eq. (21) for the asymmetry parameter. The only one unknown parameter in Eq. (21) is the effective radius of particles. Substituting the value of W presented by Eqs. (20)–(12), we arrive to a transcendent equation for the determination of a single unknown parameter (a_{ef}):

$$T(\lambda) - t(\lambda)u(\mu_0)u(\mu) = 0, \tag{23}$$

where

$$t = \frac{sinhy}{\sin h(x + ay)} \tag{24}$$
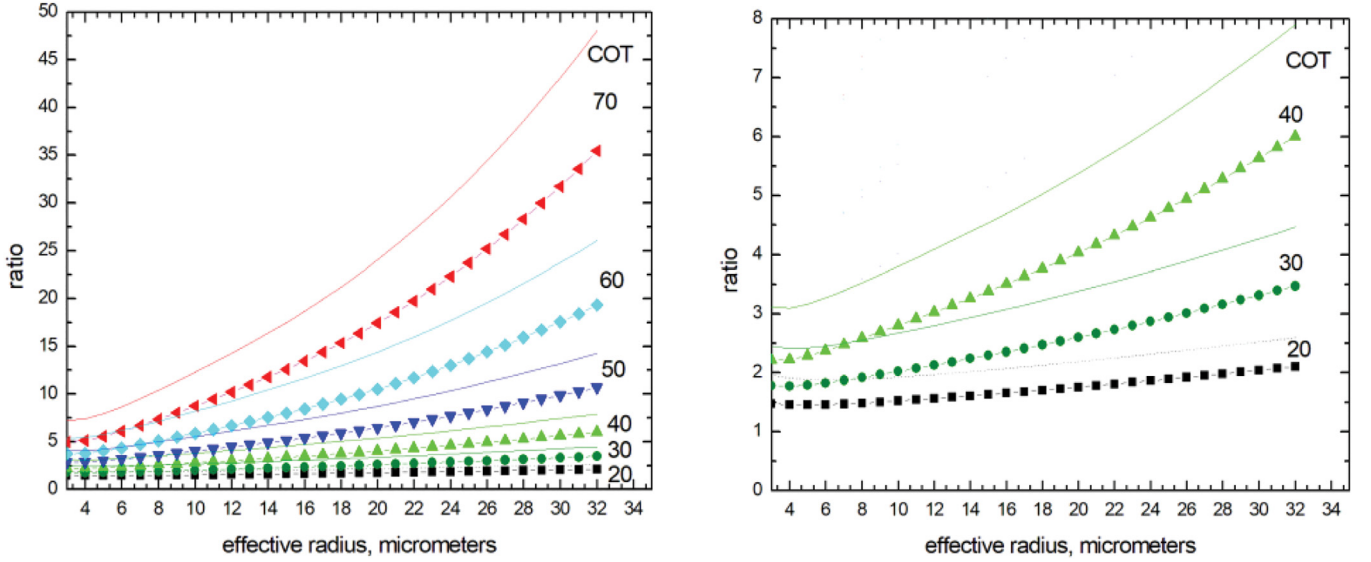
Fig. 10. The dependence of the ratio $\rho = \frac{T(1640nm)}{T(1020nm)}$ on the size of particles at several values of COT for the case of black underlying surface (symbols+lines) and the case of surface albedo $A = 0.4$ (lines). The results presented in the right panel are the same as in the left panel except just for the COTs equal to 20, 30, and 40.

is the global transmittance defined as [17]

$$t = 4 \int_0^1 d\mu_0 \int_0^1 \bar{T}(\mu_0, \mu) d\mu. \tag{25}$$

Here $\bar{T}(\mu_0, \mu)$ is the azimuthally averaged transmission function. The value of a_{ef} derived from Eq. (23) can be used to determine the liquid water path W using Eq. (22). The cloud optical thickness is found from Eq. (6).

As it was emphasized above, such an approach leads to multiple solutions (see Fig. 9). To increase the accuracy of the inverse problem solution, one must minimize the following function:

$$F(\lambda) = \frac{T_{meas}(\lambda)}{T_{meas}(\lambda_0)} - \frac{t(\lambda)}{t(\lambda_0)}, \tag{26}$$

where λ_0 is the reference wavelength (say, 1020 nm).

For instance, the dependence of the ratio $\rho = \frac{T(1640nm)}{T(1020nm)}$ on the size of particles is given in Fig. 10. It follows that this ratio can be used to derive the size of particles in unique way at COTs larger than about 20. Otherwise, multiple solutions of inverse problem are possible. Also the value of ρ can be measured with higher accuracy as compared to the value of the transmission function at a given wavelength. This leads to the increased accuracy of the inverse problem solution.

2.2.2.2. The solution of inverse problem for underlying non-black Lambertian surface. Eq. (26) is valid only for black underlying surfaces (e.g., ocean). Land surfaces often strongly reflect incoming solar light, which can be reflected again from the cloud (multiple times) thus causing an increase of the transmission function as observed by a ground instrument. This enhancement can be studied using the following approximation valid for Lambertian underlying surfaces with albedo A [17]:

$$T_{surf} = T + \frac{At(\mu_0)r_p(\mu)}{1 - Ar_s}, \tag{27}$$

where T is given by Eq. (11) and

$$r_s = \exp(-y) - t\exp(-x - y), \quad r_p(\mu)$$
$$= \exp(-yu(\mu)) - tu(\mu)\exp(-x - y), t(\mu_0) = tu(\mu_0). \tag{28}$$

It follows from Eq. (19) at SSA equal to 1:

$$T_{surf} = tu(\mu_0)u(\mu) + \frac{Atu(\mu_0)(1 - tu(\mu))}{1 - A(1 - t)}. \tag{29}$$

This enables analytical determination of global transmittance for known surface albedo A:

$$t = \frac{(1 - A)T}{(1 - A)u(\mu_0)u(\mu) + A(T + u(\mu_0))}. \tag{30}$$

Then one can derive:

$$\tau_{tr} = \frac{1}{b}(t^{-1} - a), \tau = \frac{\tau_{tr}}{\gamma}. \tag{31}$$

These equations generalize the technique of the COT determination described in the previous section on the case of reflecting underlying surfaces.

Also it follows from Eq. (26) for the cost function for multiple wavelengths:

$$F(\lambda) = \frac{T_{meas}(\lambda)}{T_{meas}(\lambda_0)} - \Phi(\lambda)\frac{t(\lambda)}{t(\lambda_0)}, \tag{32}$$

where

$$\Phi(\lambda) = \frac{1 + S(\lambda, \mu)}{1 + S(\lambda_0, \mu)} \tag{33}$$

and

$$S(\lambda) = \frac{Ar_p(\lambda, \mu)}{(1 - Ar_s(\lambda))u(\mu)}. \tag{34}$$

We show the ratio $\rho = \frac{T(1640nm)}{T(1020nm)}$ for the surface albedo equal to 0 and 0.4 in Fig. 10. It follows that the sensitivity to the ER increases with the surface albedo and COT.

2.2.2.3. Fast semi-analytical cloud retrieval technique based on measurements at three wavelengths. We apply the technique described above to the synthetic measurements of the BTF at three wavelengths: 440, 1020, and 1640 nm. Then Eq. (32) is transformed to

$$F(\lambda) = \frac{T_{meas}(1640nm)}{T_{meas}(1020nm)} - \Phi(1640nm)\frac{t(1640nm)}{t(1020nm)}. \tag{35}$$

This function depends both on ER and LWP. The LWP can be expressed via the transmission function at 440 nm (see Eq. (14)). Therefore, the effective radius is to be found from the single transcendent equation:

$$\frac{T_{meas}(1640nm)}{T_{meas}(1020nm)} - \Phi(1640nm)\frac{t(1640nm)}{t(1020nm)} = 0. \tag{36}$$

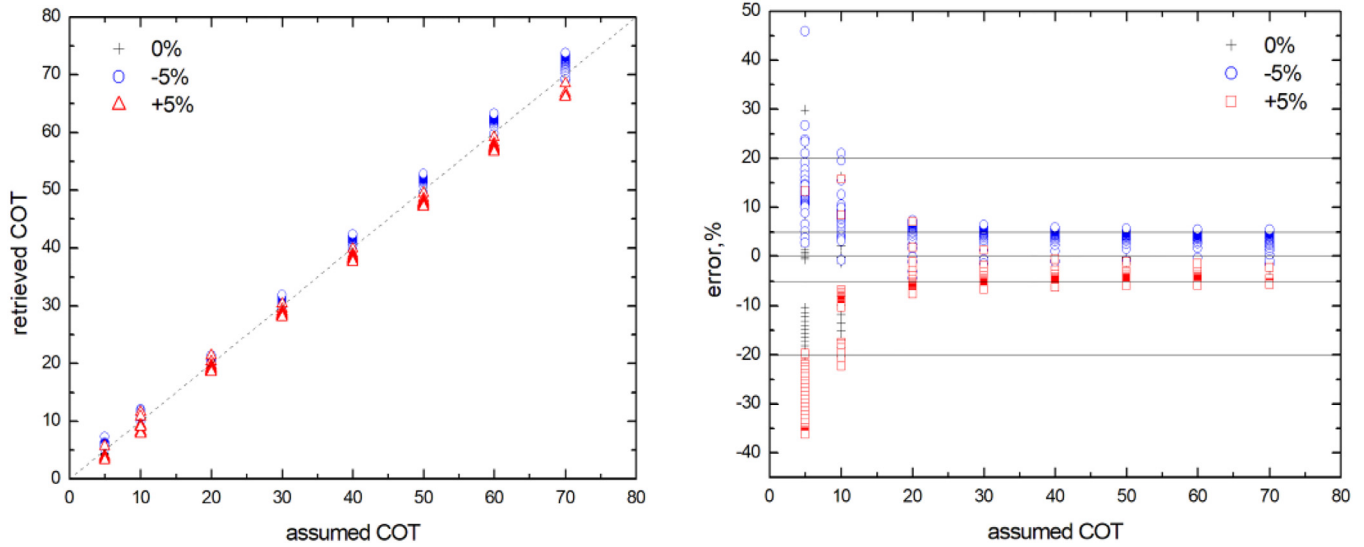**Fig. 11.** The errors of the cloud optical thickness determination for the effective radius in the range 3–33 μm as function of COT.
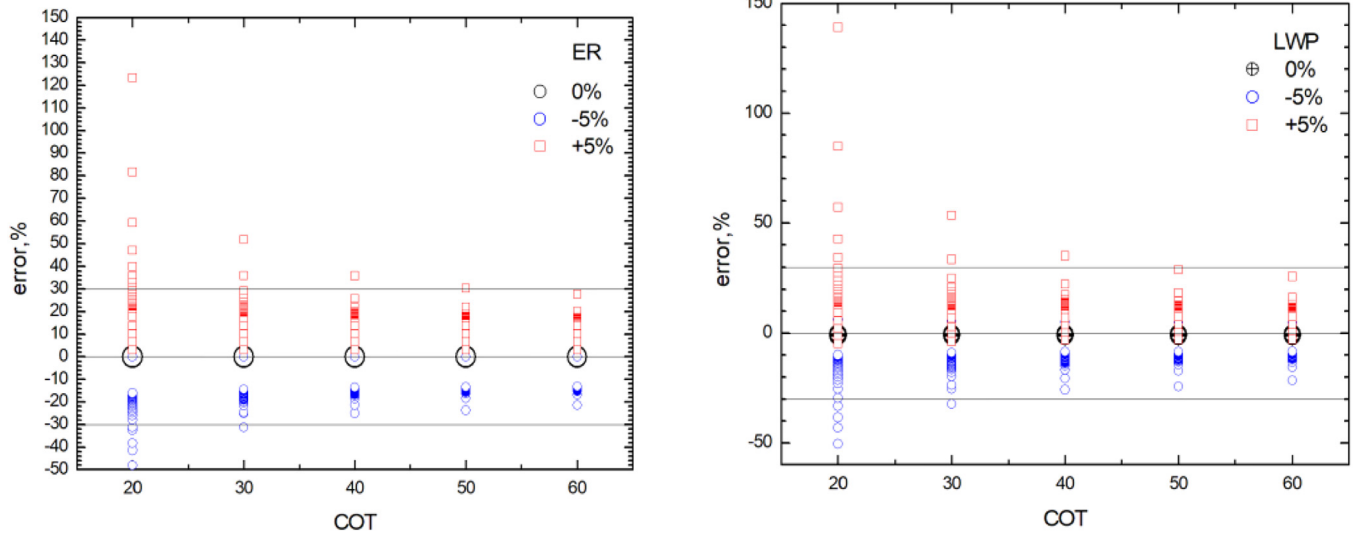

Fig. 12. The errors of the effective radius and LWP determination for the effective radius in the range 3–33 μm as function of COT.

The example of retrievals at different values of the measurement errors (0, −5%, +5%) is given in Figs. 11 and 12. The solution of Eq. (36) has been performed using the Brent's method [23]. Eq. (36) is valid at any underlying surface spectral reflectance. It has been assumed that the surface is black at 440 and 1640 nm. The contribution of surface reflectance to the detected signal under clouds is often low because the cloud tBTF is low at 1640 nm. We have assumed that the underlying surface is reflective with albedo 0.4 at 1020 nm. We conclude that COT is determined with accuracy better than 10% for COTs larger than 20 and errors of measurements below 5%. The error of retrievals can reach 30% depending on the values of ER and errors of measurements for thin clouds (at COT=5). The uncertainty of LWP and ER retrieval is better than 30% (depending on ER and error of measurements) for most of cases if COT is larger than 30. This points to the fact that the measurements of cloud transmission function must be performed with the highest possible precision.

In the next section we apply the proposed fast Semi-Analytical Retrieval technique based on cloud transMittAnce measuremenTs (SARMAT) at the triplet 440/1020/1640 nm by the CIMEL ra-

diometer. Also we compare our results to those derived from the cloud mode AERONET observations and look-up-table approach [10].

3. Application of the developed inversion scheme to experimental measurements of the solar light transmitted by a cloud layer

Sun/sky radiometer CIMEL has been deployed by AERONET since early 90 s [16]. It has 1.2° field of view and takes measurements of direct sun and diffuse sky radiances at various wavelengths within 0.34–1.64 μm spectral range. When Sun is blocked by the clouds CIMEL sun/sky radiometer switches to the "cloud mode" taking measurements of sky radiances in the zenith direction [9,10,15] . Sky measurements in the cloud mode are performed at 10 s interval for standard CIMELs and at ~35 s for the instruments with polarizers. CIMEL digital counts should be multiplied by calibration coefficients for sky channels to get the values of radiance at each channel. The calibration coefficients and also the extraterrestrial solar irradiance F_0 (see Eq. (1)) integrated over

Table 2

The values of the extraterrestrial irradiance F_0 [24] and calibration constants B for each channel for the CIMEL instrument used. The dimensionless constant $K=\pi B/F_0$ can be used to derive the transmittance from CIMEL digital counts M (namely, it follows: $T=KM/\mu_0$). The last column gives the spectral surface albedo for the GSFC AERONET (38.99 N, 76.84 W) site derived from Moderate Resolution Imaging Spectroradiometer observations [25-28]. The constants given in this Table are not universal and must be assessed for each optical instrument/site/day individually. The measurements have been performed on May 1, 2019.
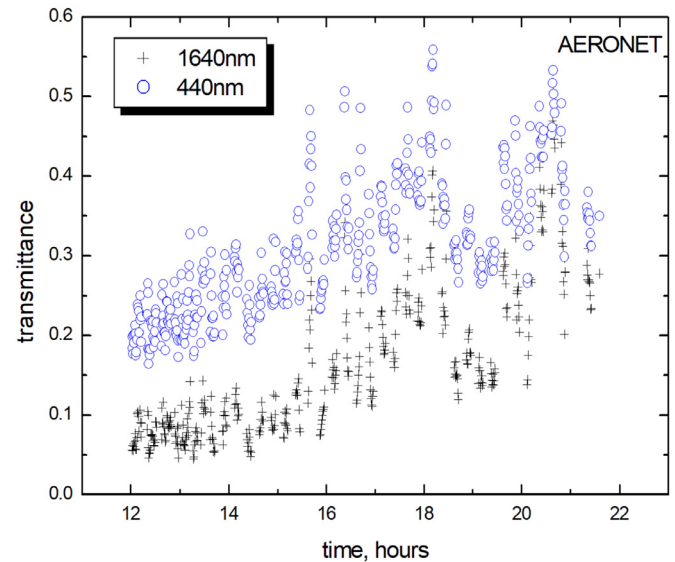
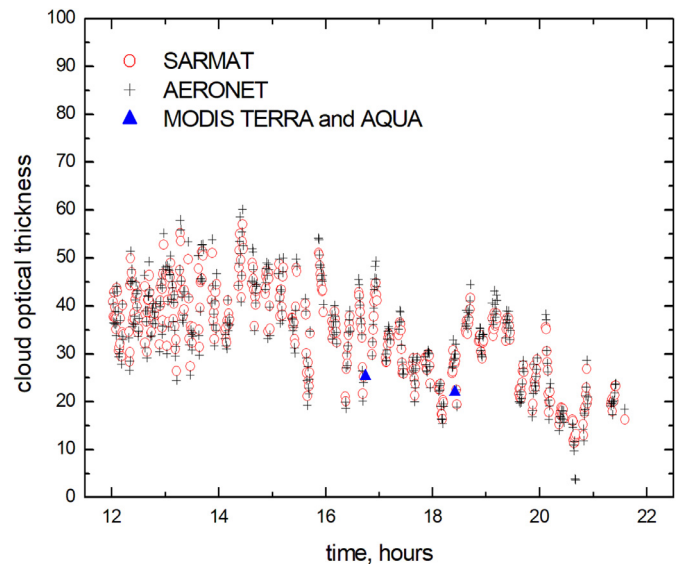| λ, μm	F_0, W/$\frac{m^2}{\mu m}$	B, W/$\frac{m^2}{\mu m}$/sr	K	A
0.440	1789.16	0.24483	4.299e-4	0.041
0.500	1948.01	0.26034	4.199e-4	0.061
0.675	1485.15	0.16531	3.497e-4	0.071
0.870	973.18	0.12438	4.016e-4	0.428
1.020	702.65	0.18957	8.484e-4	0.408
1.640	233.12	0.03233	4.359e-4	0.236
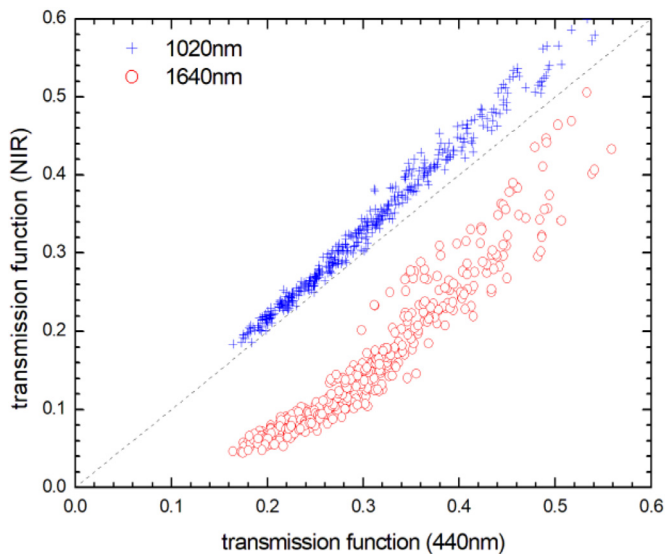
Fig. 13. The dependence of the transmission function at 1020 and 1640 nm as function of transmission function at 440 nm derived from CIMEL measurements.

Fig. 14. The dependence of transmission functions at 440 and 1640 nm on time as measured by CIMEL. Time given here and below is the Greenwich Meridian Time (GMT).


Fig. 15. The inter-comparison of current AERONET cloud mode COT and one retrieved from the fast asymptotic radiative transfer algorithm. Values from the MODIS cloud product for Terra and Aqua are also shown.

filter spectral function for each channel are given in Table 2. We also show the spectral albedo estimated using MODIS measurements in Table 2.

The dependence of measured transmission function at the near IR wavelengths at the transmission function at 440 nm is shown in Fig. 13. It follows that $T(1020$ nm$)$ is almost linear function of $T(440$ nm$)$. This is not the case for the $T(1640$ nm$)$. The transmission function value at 1640 nm has risen from 0.05 till 0.5 during the experiment (see Fig. 14). There is also the trend for the increase of $T(440$ nm$)$ with time (see Fig. 14). This points to the fact that the COT had decreased with time over AERONET site location considered in this paper. The retrieved COT using the technique described in this paper (see Eq. (21)) at three wavelengths (440/1020/1640 nm) with account for the surface reflectance (see Table 2) is shown in Fig. 15 together with the COT retrieved using standard AERONET cloud mode retrieval techniques based on the look-up-table approach. One can see that the COT is generally decreasing with time, as one may expect (see Fig. 14). The difference between two retrievals is below 10% (see Fig. 16), which is an excellent result taking into account that the current AERONET cloud mode COT retrieval is characterized by the 18% retrieval uncertainty. Also different wavelengths are used in the retrieval process (670/875 nm for the standard AERONET cloud mode retrieval and 440/1020/1640 nm for our fast retrieval technique). The retrieved

LWP and ER in the framework of SARMAT is given in Figs. 17 and 18. It follows that the average radius of droplets during the observational time was 9.8 μm with the standard deviation (STDV) 3.4 μm. Both ER and LWP decrease with time with average LWP equal to 183.3 g/m^2 and STDV=82.1 g/m^2. The coefficient of variance (STDV/average, see Table 3) was similar for COT, ER, and transmission function at 440 nm and 1020 nm (about 30%). The coefficient of variance of T(1640 nm) and LWP was a bit larger (see Table 3). The results of satellite retrievals (MOD06 product) of the respective cloud parameters are shown in Table 3. We see that ground and satellite data provide similar results – especially taken into account different spatial scales of ground and satellite measurements (couple of meters for low cloudiness existing at the time of measurements, see https://mplnet.gsfc.nasa.gov/) and 1 km satellite retrievals.
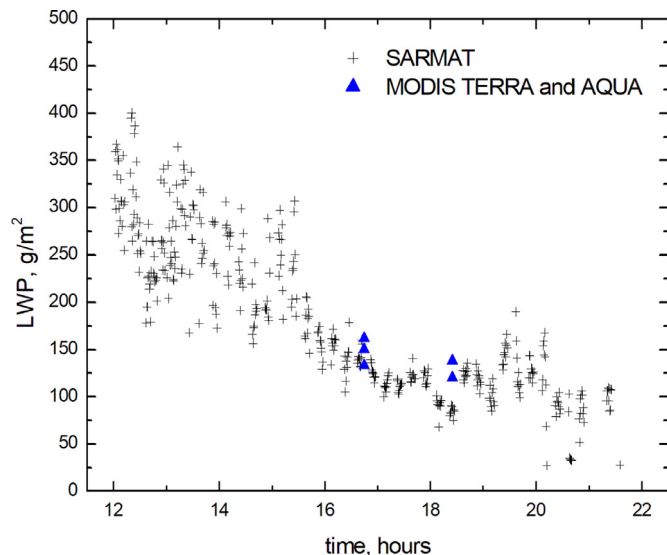
Table 3

The statistics of retrieved cloud parameters and measured transmission functions at 440, 1020, and 1640 nm. We also show the results of retrievals based on satellite MODIS Terra (38.987 N, 76.851 W, 16:45 GMT) and Aqua (38.998 N, 76.883 W, 18:25GMT) observations. Good agreement between satellite and averaged ground observations is found, although the spatial scale of satellite (1 km) and ground (several squared meters) observations is quite different. Different COTs, ERs, and LWPs for Terra and Aqua due to different near-infrared wavelengths (1.6, 2.2, and 3.7 μm) used in the retrieval process for the assumed vertically homogeneous clouds although real – world clouds are vertically inhomogeneous turbid media.
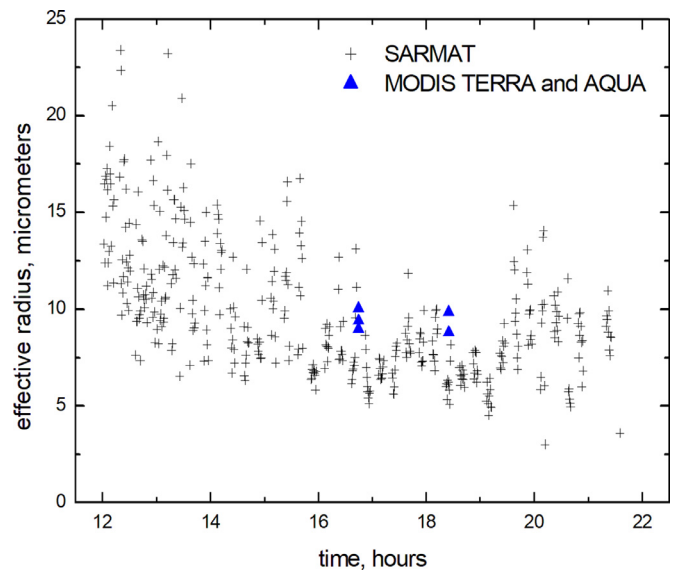
Parameter	Average	Standard deviation	Coefficient of variance	Terra MODIS retrievals	Aqua MODIS retrievals
COT	34.3	2.8	0.27	24.84	–
				25.16	21.58
				25.36	22.02
ER, microns	9.8	9.4	0.29	8.98	–
				9.4	8.81
				10.05	9.85
LWP, g/m^2	183.3	82.1	0.45	133.0	–
				150.0	120.0
				162.0	138.0
T(440 nm)	0.307	0.085	0.28	–	–
T(1020 nm)	0.336	0.097	0.29	–	–
T(1640 nm)	0.163	0.096	0.59	–	–
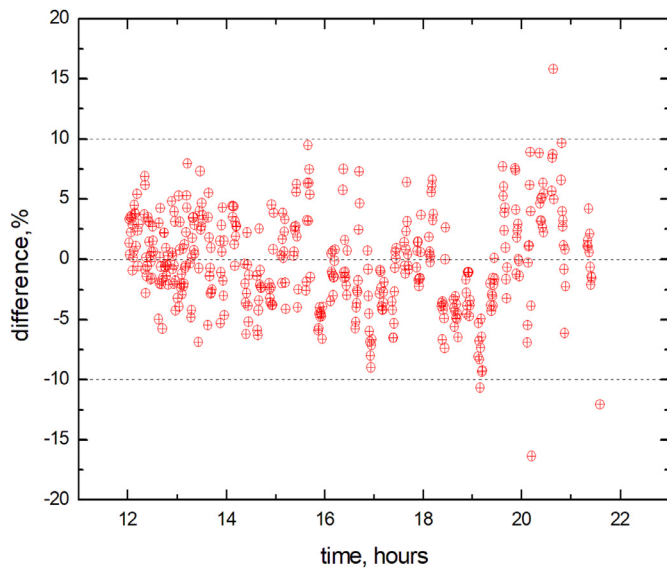
Fig. 16. The time series of difference between AERONET cloud mode COT and one retrieved from the fast asymptotic radiative transfer algorithm.

Fig. 18. The time series of effective radius as derived from CIMEL measurements. The results derived from satellite measurements are also shown.

Fig. 17. The time series of LWP as derived from CIMEL measurements. The results derived from satellite measurements are also shown.

4. Conclusion

In this work we have proposed a simple technique to retrieve the optical thickness, reduced optical thickness, liquid/water path, and effective radius of droplets/crystals of optically thick clouds from CIMEL observations at 440/1020/1640 nm in the assumption that clouds are vertically and horizontally homogeneous and have cloud optical thickness above 10 or so. The technique has been applied to the CIMEL observations and close correspondence with CIMEL cloud mode measurements have been found. The algorithm described above can be applied if the radiative transfer in cloud occurs in the asymptotic regime. The standard AERONET cloud mode retrieval also is applicable for the broken cloud conditions, which is not the case for the algorithm described in this paper. The occurrence of asymptotic regime, where the accuracy of SARMAT is highest, can be detected by performing the following tests:

(1) the BTF measurements in the principal plane follow the angular pattern described by Eq. (4) (cosine law) and there is no transmittance enhancement in the direction of Sun obscured by a cloud;

(2) the almucantar measurements show that there are no az-
imuthal variations of the transmitted solar light under the
cloud.

Another possibility with respect to the quantification of the ra-
diative transfer regime in cloud is the use of a lidar. Basically, our
technique can be applied if the ground-based lidar return from
upper cloud boundary is weak or not existent. Lidar polarization
ratio can be used to distinguish water/ice clouds. Also lidar mea-
surements can be used to get the cloud optical thickness for thin
clouds not covered by the technique described in this paper.

Our technique can be used to retrieve the properties of mixed
clouds as well. However, the results (except for the transport op-
tical thickness) will be biased unless *a priori* information on the
percentage of ice phase in a cloud is known or retrieved from in-
dependent measurements.

Declaration of Competing Interest

None.

Acknowledgments

Supplementary materials

Supplementary material associated with this article can be
found, in the online version, at doi:10.1016/j.jqsrt.2020.107008.

References

[1] Stephens GL, Kummerow C. The remote sensing of clouds and precipitation from space: a review. J Atmos Sci 2007;64(11):3742–65.
[2] Yershov OA, Lamden KS, Levin IM, Salganik IN, Shifrin KS. Determination of the optical thickness of clouds above the sea from brightness measurements. Izvestiya Atmosph Ocean Phys 1988;24(5):396–400.
[3] Yershov OA, Levin IM, Salganik IN, Sheberstov SV. Optical thickness of clouds over the sea. Izvestiya Atmosph Ocean Phys 1991;27(6):471–4.
[4] Leontieva E, Stamnes K. Estimations of cloud optical thickness from ground-based measurements of incoming solar radiation in the Arctic. J Climate 1994;7:566–78.
[5] Leontieva E, Stamnes K. Remote sensing of cloud optical properties from ground-based measurements of transmittance: a feasibility study. J Appl Meteorology 1996;35:2011–22.
[6] Marshak A, Knyazikhin Y, Davis AB, Wiscombe WJ, Pilewski P. Cloud-vegetation interaction: use of normalized difference cloud index for estimation of cloud optical thickness. Geophys Res Lett 2000;27(12):1695–8. doi:10.1029/1999GL010993.
[7] Marshak A, Knyazikhin Y, Evans KD, Wiscombe WJ. The "RED versus NIR" plane to retrieve broken-cloud optical depth from ground-based measurements. J Atmos Sci 2004;61:1911–25 2004.
[8] Kikuchi N, Nakajima T, Kumagai H, Kuroiwa H, Kamei A, Nakamura R, Nakajima TY. Cloud optical thickness and effective particle radius derived from transmitted solar radiation measurements: comparison with cloud radar observations. J Geophys Res 2006;111:D07205. doi:10.1029/2005JD006363.
[9] Chiu JC, Marshak A, Knyazikhin Y, Wiscombe WJ, Barker HW, Barnard JC, Luo Y. Remote sensing of cloud properties using ground-based measurements of zenith radiance. J Geophys Res 2006;111:D16201. doi:10.1029/2005JD006843.
[10] Chiu JC, Huang CH, Marshak A, Slutsker I, Giles DM, Holben BN, Knyazikhin Y, Wiscombe WJ. Cloud optical depth retrievals from the Aerosol Robotic Network (AERONET) cloud mode retrievals. J Geophys Res 2010;115:D14202 2010. doi:10.1029/2009JD013121.
[11] Chiu JC, Marshak A, Huang CH, Várnai T, Hogan RJ, Giles DM, Holben BN, O'Connor EJ, Knyazikhin Y, Wiscombe WJ. Cloud droplet size and liquid water path retrievals from zenith radiance measurements: examples from the Atmospheric Radiation Measurement Program and the Aerosol Robotic Network. Atmos Chem Phys 2012;12:10313–29. doi:10.5194/acp-12-10313-2012.
[12] Kokhanovsky AA, McBride PJ, Schmidt KS, Pilewskie P. The determination of cloud optical thickness and effective particle size from measurements of transmitted solar diffuse light. IEEE Geosci. Remote Sens. Lett. 2013;10:1512–16. doi:10.1109/LGRS.2013.2261274.
[13] Brückner M, Pospichal B, Macke A, Wendisch M. A new multispectral cloud retrieval method for ship-based solar transmissivity measurements. J Geophys Res Atmos 2014;119:1–17. doi:10.1002/2014JD021775.
[14] LeBlanc SE, Pilewskie P, Schmidt KS, Coddington O. A spectral method for discriminating thermodynamic phase and retrieving cloud optical thickness and effective radius using transmitted solar radiance spectra. Atmos Meas Tech 2015;8:1361–83. doi:10.5194/amt-8-1361-2015.
[15] Shonk JKP, Chiu JC, Marshak A, Giles D M, Huang CH, Mace GG, Benson S, Slutsker I, Holben BN. The impact of neglecting ice phase on cloud optical depth retrievals from AERONET cloud mode observations. Atmos Meas Tech 2019;12:5087–99. doi:10.5194/amt-12-5087-2019.
[16] Holben BN, Eck TF, Slutsker I, Tanre D, Buis JP, Setzer A, Vermote E, Reagan JA, Kaufman Y, Nakajima T, Lavenu F, Jankowiak I, Smirnov A. AERONET - A federated instrument network and data archive for aerosol characterization. Rem. Sens. Env. 1998;66:1–16.
[17] Kokhanovsky A. Cloud optics. Berlin: Springer; 2006.
[18] Sobolev VV. Light scattering in planetary atmospheres. Pergamon Press: Amsterdam: Pergamon; 1975. p. 275.
[19] Korkin S, Lyapustin A. Matrix exponential in C/C++ version of vector radiative transfer code IPOL. J Quant Spectrosc Radiat Transf 2019;227:106–10.
[20] Henyey LG, Greenstein JL. Diffuse radiation in the Galaxy. Astrophys J 1941;93:70–83. doi:10.1086/144246.
[21] Korkin S, Lyapustin A, Rozanov V. Modifications of discrete ordinates method for computations with high scattering anisotropy: comparative analysis. J Quant Spectrosc Radiat Transf 2012;113:2040–8.
[22] Emde C, Barlakas V, Cornet C, Evans F, Korkin S, Ota Y, Labonnote LC, Lyapustin A, Macke A, Mayer B, et al. IPRT polarized radiative transfer model intercomparison project—Phase A. J Quant Spectrosc Radiat Transf 2015;164:8–36.
[23] Brent RP. Algorithms for minimization without derivatives. Englewood Cliffs, New Jersey: Prentice-Hall; 1973.
[24] Coddington O, Lean J L, Pilewskie P, Snow M, Lindholm D. A solar irradiance climate data record. Bull Am Meteorol Soc 2016;97:1265–82.
[25] Wang Z, Schaaf CB, Sun Q, Shuai Y, Roman MO. Capturing rapid land surface dynamics with Collection V006 MODIS/BRDF/NBAR/Albedo (MCD43) product. Remote Sens. Environ. 2018;207:50–64.
[26] Sinyuk A, Holben BN, Eck TF, Giles DM, Slutsker I, Korkin S, Schafer JS, Smirnov A, Sorokin M, Lyapustin A. The AERONET Version 3 aerosol retrieval algorithm, associated uncertainties and comparisons to Version 2. Atmos Meas Tech Discuss 2020 in review. doi:10.5194/amt-2019-474.
[27] Platnick S, Meyer K, King M D, Wind G, Amarasinghe N, Marchant B, et al. The MODIS cloud optical and microphysical products: collection 6 updates and examples from Terra and Aqua. IEEE Trans Geosci Remote Sens 2017;55:502–25. doi:10.1109/TGRS.2016.2610522.
[28] MODIS BRDF/Albedo/NBAR Product MCD43 https://www.umb.edu/spectralmass/terra_aqua_modis/modis_brdf_albedo_product_mcd43.